Authors preprint of paper published as Nuclear Fusion 54 (2014) 083001

Effect of Beryllium on the Deuterium Implantation in Tungsten by Atomistic Simulations

A. Lasa, K. Heinola and K. Nordlund

Association Euratom-Tekes – Department of Physics, P.O. Box 43, FI-00014 University of Helsinki, Finland

E-mail: ane.lasa@helsinki.fi

Abstract.

Tungsten (W) and beryllium (Be) have been chosen as plasma facing materials for the ITER reactor and the main fuel component will be deuterium (D). Due to plasma-wall interactions, these materials will immediately mix via erosion, transport and re-deposition. We present the first atomistic study on the effect of D co-implanted with Be into W, by modelling D plus Be irradiation of W surfaces, at projectile energies and compositions relevant for the plasma-wall interactions. The D implantation and Be sticking yields increased with the Be fraction in the system, especially at the lowest energies, as a Be layer deposited on the surface. Tungsten was sputtered by Be, although the yield was partially suppressed by the deposited Be-D layer, and the Be erosion was determined by the balance between the Be concentration at the surface and projectile energy. Also molecules were sputtered: a large fraction of the D is reflected as D_2, and purely metallic molecules (Be_2, BeW), as well as different Be-D compounds were sputtered. On the other hand, the D clustered when implanted in or beneath a pre-deposited Be-W layer.

PACS numbers: 28.52.Av, 28.52.Fa, 31.15.xv

1. Introduction

ITER aims to be the first experimental fusion reactor reaching ignition [1]. Due to its design, the plasma conditions (e.g., temperature, particle flux and thermal loads) and thus the plasma facing material requirements, vary with location in the reactor. Any plasma-wall interaction driven unexpected effect, such as melting, excessive erosion or fuel retention, could be the show-stopper for ITER. Tungsten (W) will be used for the divertor area and the main wall of the reactor will be made of beryllium (Be). Erosion, transport and subsequent re-deposition may lead to mixing of these materials, calling for a complete understanding of the interplay between the plasma particles (e.g., deuterium, D) not only with the pure materials, but also their mixtures. Furthermore, W and Be may form alloys [2], increasing the complexity of the processes involved.

An extensive experimental work on the W-Be-D interactions can be found in the literature. For example, W was exposed to Be-seeded D and D_2 plasmas [3, 4, 5, 6, 7], to particularly study the effect of Be on the D retention in W. Also, based on these experiments, a particle balance model was developed to determine the critical Be concentration in a plasma at which a Be layer grows instead of being re-eroded [5]. Further, an empirical scaling equation was suggested describing the influence of the co-deposition conditions (surface temperature, incident particle energy and flux) on the D retention [8]. However, the computational work is scarce, only consisting of Monte Carlo simulations on the erosion of W and carbon exposed to Be-seeded D plasmas [9], a comparison between Binary Collision Approximation [10] and Molecular Dynamics (MD) simulations on the mixed layer erosion [11] and MD modelling of W-Be mixed layer formation [12] and Be erosion from Be_2W surfaces under D irradiation [13].

In this work, we present a systematic study of W−Be−D interactions at the atomic scale. The Be-seeded D irradiation of W surfaces was simulated with MD, varying the Be fraction among the projectiles, as well as the impacting energies. As complementary cases, different amorphous W-Be mixtures were exposed to pure D irradiation.

MD is a computational method working on the atomistic scale and thus, a suitable tool to study the material mixing, particle reflection and in general low-energy irradiation effects in materials, including chemical effects. However, the MD results cannot always be compared directly to experiments due to different time-scales (ns in MD vs s in experiments). Due to the short simulation time-scale, MD does not account for processes such as long-range diffusion, an important mechanism e.g., for the D retention in fusion reactors and alloy formation at W−Be interfaces [14, 15]. To overcome this limitation and directly compare the modelling to the experimental data, our results will be provided to larger-scale computational methods, such as rate equation theory codes [16] for studying the retention in mixed materials at time-scales of a plasma discharge, and to codes tracing the impurity transport in a reactor [17] or erosion-deposition patterns on the walls [18], for a more accurate description of the plasma-wall interactions.

The article is structured as follows. The simulation methods used in this work,

including the details of each studied case, are introduced in section 2. The results and their interpretation are given in the section 3. In 3.1, the results from the simultaneous D-Be irradiation are presented, including the structure modifications, projectile implantation characteristics and layer erosion. In 3.2 the main outcome from the consecutive and non-cumulative irradiation is shown and compared to the simultaneous irradiation results. In 3.3, the outcome of the present work is compared to other computational and experimental studies, including the connection to possible mechanisms suppressing the D bubble formation by Be-seeding of the plasma. Finally, the main results are summarized.

2. Method

The simulations were performed using the MD code PARCAS [19]. A reactive bond order potential, modified to include a more accurate description of the W−W interactions was used to calculate the W−Be−D interactions [20, 21].

The MD simulations were performed in two main steps. First, an initial BCC structure for pure W was relaxed at 500 K, including the opening of the (100)-oriented W surface. Further details regarding these relaxations can be found in Ref [22]. Secondly, the relaxed W surface was irradiated with different D−Be mixtures, choosing randomly an atom type at a time, with impacting energies ranging from $10-150$ eV and with Be fractions among the projectiles ranging from $2-66\%$. We will refer to these simulations as *simultaneous irradiation*. Each case consisted of 4000 cumulative, mono-energetic impacts at normal incidence, using the same energy for either projectile type. At 150 eV, 3000 impacts were simulated. A new projectile impacted every 7 ps: for the first 2 ps the temperature within 3 Åof the cell boundaries in x and y was cooled towards 500 K. The time 2 ps was chosen such that most of the high-energy interactions took place during this time, e.g. 99.99% of the particle reflection for 100 eV impacts in the cells with $2-66\%$ of Be. During the next 5 ps, the whole cell was cooled down to 500 K in order to remove the energy introduced by the ion. The Berendsen thermostat was used for the temperature control, with a cooling constant of $\tau = 100$ fs. Between impacts, the cell was randomly shifted in the x and y directions, so that each new projectile would impact on a new surface location and the entire surface will be evenly irradiated. This led to a flux of $\sim 10^{28}$ $\mathrm{m^{-2}s^{-1}}$, a fluence of $4 \cdot 10^{20}$ $\mathrm{m^{-2}}$and a total simulation time of 28 ns. These initial cells contained 3000 W atoms, held in a volume of $3.1 \times 3.1 \times 3.7$ $\mathrm{nm^3}$ and were used for impacting energies of $10-50$ eV. For irradiation at 100 and 150 eV, a 3600 or 4800 W atom cell was used, with a cell depth of 4.7 or 5.7 nm, respectively.

In what follows, unless another range is explicitly mentioned, we will refer to the irradiation ≤ 50 eV as *low energy*, and to the impacts at ≥ 100 eV as *high energy*. *Low fraction* will be used for projectile compositions with $\leq 10\%$ Be, and *high fraction* above it ($\geq 33\% Be$).

In addition to the simultaneous Be-D impacts, D irradiation of pre-formed W-Be mixed layers was studied. The substrate for the cumulative D impacts was formed

depositing Be with 50 eV on W (3000 Be impacts, at normal incidence). A detailed description of this material mixing is given in [12]. The W−Be mixture was repeatedly quenched (heated up to 1000 K and cooled down to 500 K) until the system was energetically stable. Finally, this substrate was exposed to 3000 cumulative D impacts with energies ranging 10−100 eV. Thus, we will refer to these simulations as *consecutive irradiation*.

Further, non-cumulative D impacts on different amorphous W-Be mixtures were simulated to obtain more accurate statistics of the D and Be reflection yields. These simulations are referred as *non-cumulative irradiation*. The amorphous cells were created by randomly placing 3000−4800 atoms in a $3.2 \times 3.2 \times 4.0$ nm^3 cell, at least 2 Å apart, at the desired W:Be ratio; 2:1 (W_2Be), 1:1 (WBe) or 1:2 (WBe_2). To obtain an energetically stable cell, the W−Be mixtures were repeatedly quenched (heated up to 2000 K, kept at that temperature for 20 ps, cooled down to 500 K at a rate of 0.05 K/fs and kept at 500 K for 30 ps) until the potential energy remained constant. Finally, we simulated 10000 non-cumulative D impacts on each of the surfaces with D energies varying $10 - 200$ eV. A more detailed description of these simulations can be found in [11].

The different set-ups of the simulations (D−Be percentages, their energies and the substrate compositions) are summarized in Table 1. A more thorough description of the simulation parameters, such as temperature and pressure control, treatment of sputtered and backscattered species, use of the periodic boundary conditions and electronic stopping, can be found in Ref. [22].

3. Results and discussion

3.1. Simultaneous Be-D irradiation on W

3.1.1. Structure modification by the simultaneous Be-D irradiation The cumulative Be-seeded D irradiation led to the formation of different morphologies. At the lowest energies ($10 - 30$ eV) the Be was deposited on W forming clear W-Be-D interfaces (Fig. 1, a). In contrast, at higher energies ($50 - 150$ eV) the Be atoms reached deeper W layers leading to a larger material mixing (Fig. 1, b). On the other hand, in absence of a deposited Be layer (low Be fractions), the D was implanted in interstitial positions of the W lattice. Due to the high flux, the D concentration in W was super-saturated, forming edge dislocation planes to release the stress in the W matrix (Fig. 1, c). Further, the topmost layers also changed their structure, forming for instance, rough Be-D surfaces (Fig. 1, a), dangling Be-D clusters (Fig. 1, d) and amorphous W surfaces (Fig. 1, e).

3.1.2. Implantation during the simultaneous Be-D irradiation The Be reflection yields (Fig. 2 right) hardly changed with the Be fraction at high energies due to the invariant

Table 1. Characteristics of the cumulative Molecular Dynamics simulations. *irradiation* refers to either cumulative (*cum*) or non-cumulative (*non-cum*) impacts, *ion species* are the impacting species and their percentages, *substrate* refers to the initial cells composition: *a-* is amorphous, *sc-* single-crystal and *d-* pre-deposited. *energies* are the impacting energies simulated in each case.

irradiation	ion species		substrate	energies (eV)
	$Be(\%)$	$D(\%)$		
cum.	2	98	sc-W	$10, 30, 50, 100, 150$
cum.	10	90	sc-W	$10, 30, 50, 100, 150$
cum.	33	66	sc-W	$10, 30, 50, 100, 150$
cum.	66	33	sc-W	$10, 30, 50, 100, 150$
cum.	–	100	d-WBe	$10, 30, 50, 100$
non-cum.	–	100	a-W_2Be	$10, 50, 100, 200$
non-cum.	–	100	a-WBe	$10, 50, 100, 200$
non-cum.	–	100	a-WBe_2	$10, 50, 100, 200$

surface composition. In contrast, at low energies, the Be was deposited on the W surface. At high Be concentrations, a Be layer was quickly formed on the surface. The layer growth rate increased during the irradiation due to the higher Be sticking coefficient on Be than on W, which agrees with other computational studies [9].

On the other hand, the D implantation (Fig. 2 left) increased with the impacting energy, as also predicted by binary collision approximations (e.g., TRIM [23]). Small differences arose in the MD reflections yields when varying the ion composition. In general, D shows a lower reflection yield from Be surfaces than from W [24, 25, 26], leading to an over all decrease of the yield with increasing the Be concentration if a Be layer is formed at the surface. In greater detail, a Be-rich layer grew on the surface at low energies ($30 - 50$ eV), with a growth rate increasing with the Be fraction. As D was implanted in a narrow depth range, its concentration in the Be-rich layer saturated quicker for the lowest layer growth rates, leading to an increase in the D reflection. In contrast, at high energies the topmost surface composition hardly varied throughout the irradiation as no Be layer was formed. Also, the large implantation range prevented any D saturation within the fluence modelled here. Thus, the reflection yields remained independent from the ion composition. On the other hand, at the lowest energy (10 eV) the projectiles remained at the surface, the D surface saturation was reached even for the highest Be concentrations and the D reflection yields converged.

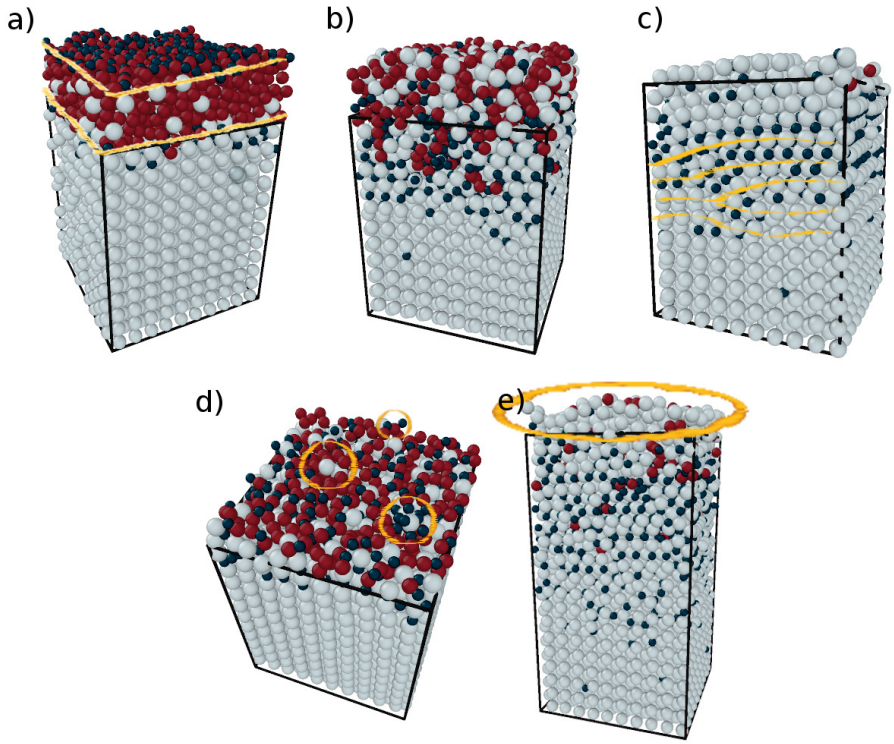

Figure 1. Examples of different structures formed after the simultaneous Be-D irradiation. The W atoms are show in light gray, the Be in red and D in dark blue. The main feature of each structure is highlighted in yellow. a) clear W-Be-D interfaces at high Be fractions and low irradiation energies (33% Be, 10 eV); b) mixed W-Be-D layers at high Be fractions and intermediate or high energies (33% Be, 50 eV); c) dislocation planes formed at the lowest Be concentrations (2% Be, 50 eV); d) cluster formation at the surface at low irradiation energies and intermediate Be-D fractions (10% Be, 10 eV); e) amorphous W-like surface at high energies (10% Be, 100 eV).

3.1.3. Depth profiles after the simultaneous Be-D irradiation The depth profiles of the irradiated cells also revealed the implantation characteristics described above (3.1.2).

The Be depth profiles (Fig. 3, top), when normalized to the Be fraction, showed the same shape for all the Be concentrations at high energies. In contrast, at low energies, a Be layer was deposited on the W surface. The layer growth rate, and thus the Be profile width, increased with the Be fraction among the projectiles.

Also the D depth profiles (Fig. 3, bottom) showed an invariant trend with respect to the projectile composition at high energies. However, at low energies, the subsurface D profile exhibited a *tail* towards the deposited mixed layer caused by the simultaneous Be layer growth (Be fraction $\geq 33\%$). This effect was enhanced by the D being implanted shallower in the mixed W−Be layer than in pure W or Be. For instance, TRIM [23] calculations run with the densities and W:Be ratios taken from MD, at 50 eV, result in implantation depths of 13 ± 7 Å for the mixed layer and 20 ± 11 Å for pure W or Be.

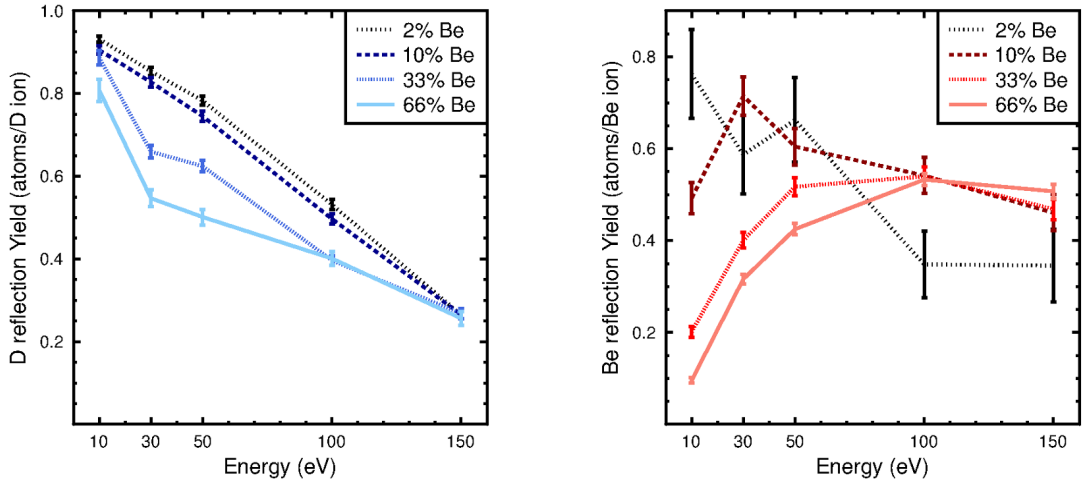

Figure 2. The D (left) and Be (right) reflection yields as a function of the projectiles energy for different projectile compositions after 4000 Be-D impacts on W surfaces (simultaneous irradiation). The Be fraction among the projectiles (in %) is given in the figure key. Note that the yields are scaled according to the projectile composition.

3.1.4. Layer erosion during the simultaneous Be-D irradiation The mixed layers described above were also eroded by the subsequent impacts, including Be, W and molecular sputtering.

The Be erosion yields (Fig. 4 left) increased with the Be concentration at the surface, and therefore, the fraction of Be among the projectiles. The yields peaked at $\sim$ 50 eV, i.e., the highest impacting energy within the Be layer deposition regime. At 10 eV, although a Be layer was formed, the low energy of the subsequent projectiles led to much lower Be sputtering yields. At high energies, the incoming Be atoms were implanted beneath the W surface. Thus, the Be concentration at the topmost surface and the Be sputtering yields decreased. The large Be erosion, in general, is likely caused by the short relaxation time between impacts for the deposited atoms.

Further, our simulations confirmed that within the energy range considered here, the W is sputtered by Be (Fig. 4 right). However, this erosion was partially balanced by the Be layer deposition, which suppressed the W sputtering [12], causing similar yields for high Be fractions ($\geq$ 33% Be).

Also molecules were found to sputter due to the simultaneous Be-D irradiation. The molecular sputtering in general (e.g., D_2, BeD_n, or Be_2 erosion) strongly depended on the Be surface concentration and contribution from the Be impacts. On one hand, a large fraction of the D was reflected as D_2 (Fig. 5, left) when Be was the dominant species at the surface ($\geq$ 33% Be, $\leq$ 50 eV). This highlights the low D_2 formation in W (observed for low Be concentrations), showing that D_2 formation is not caused by purely ballistic collisions but has a chemical component. At high energies, the projectiles were implanted deeper and in a wider depth range. Thus, the D and Be concentrations in

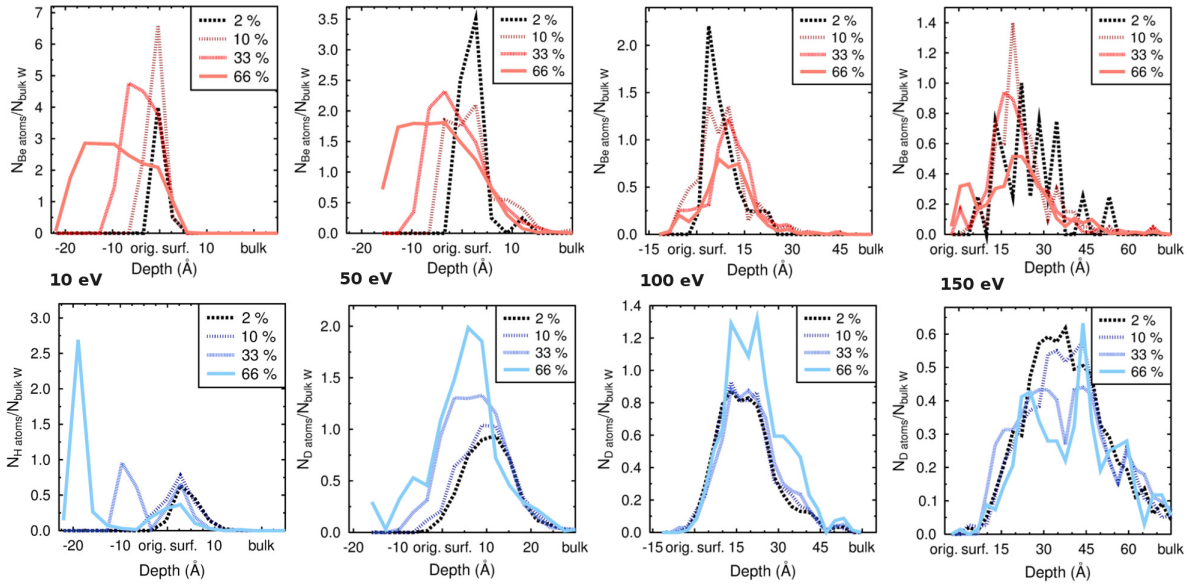

Figure 3. The Be (top) and D (bottom) depth profiles, from 10 eV (left) to 150 eV (right), for different Be concentrations, from 2% Be in black to 66% Be in light red (top) or light blue (bottom). The zero is located at the original surface and the positive z axis is towards the bulk. The depth profiles are normalized to the atomic density of the original cell (BCC W lattice), and calculated every 3.1 Å (layer width in depth), to obtain a flat profile for bulk W. All the profiles are scaled to account for the projectile composition. The statistical errors – not shown for clarity – lay between 0.005 and 0.09, as calculated for the lowest and highest concentrations, respectively.

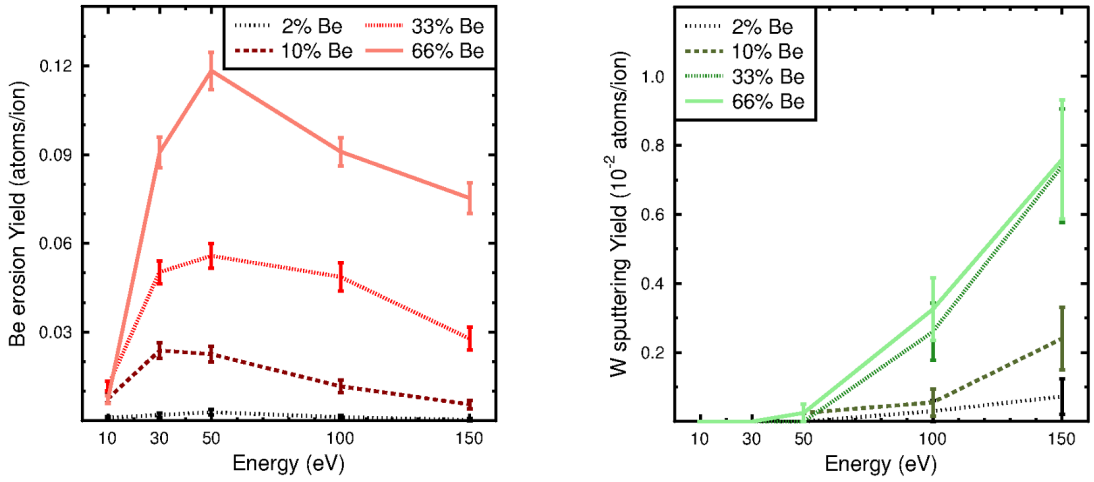

Figure 4. Be (left) and W (right) erosion yields as a function of the ion energy for different projectile compositions, after 4000 cumulative impacts (simultaneous irradiation). The Be fraction among the projectiles (in %) is given in the figure key.

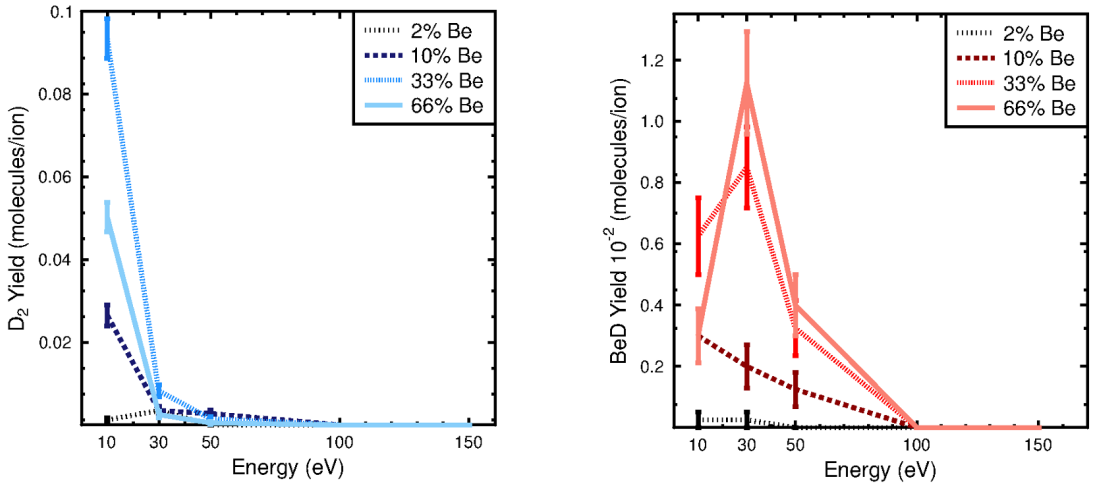

Figure 5. D_2 (left) and BeD (right) molecule sputtering yields as a function of the impacting energy for the different projectile compositions (simultaneous irradiation). The Be fraction among the projectiles (in %) is given in the figure key.

the matrix, and consequently probabilities for D_2 formation and release, were lower. On the other hand, pure metallic molecules were eroded for the high Be fraction cases. Be_2 molecules sputtered chemically and BeW physically, by dimer sputtering. Further, a wide variety of Be-D molecules were released. The Be impacts on a D-rich surface were the main BeD erosion source at high Be concentrations (compared to D impacts on the Be-rich surface), as both processes may occur but the latter requires a higher impacting energy. Due to the low impacting energy required for the former process, the BeD erosion peaked at lower energies ($\sim$ 30 eV; Fig. 5, right) and the yields were higher than for D irradiation of Be surfaces [27]. Further, for low Be fractions the BeD erosion −as the Be concentration at the topmost layers− decayed with the increase of the projectiles energy. Other Be-D species were also found to sputter, although seldom: a single Be_2D and 6 BeD_2 molecules were released. Therefore, the BeD erosion yields were also affected by the D surface concentration.

3.2. D irradiation on W-Be mixtures

3.2.1. Implantation by consecutive Be-D irradiation The reflection yields from the consecutive irradiation at low energies ($\leq$ 30 eV; Fig. 6, left) are similar to those from the simultaneous irradiation. On the other hand, the non-cumulative irradiation at low energies led to lower D reflection yields, as the surface D concentration did not get saturated. All the reflection yields (from the simultaneous, consecutive and non-cumulative irradiation) converged at high energies, as the D surface concentration did not saturate and the topmost layer composition varied the least. This lower reflection yield lead to D cluster formation and growth for the consecutive irradiation at higher energies (see

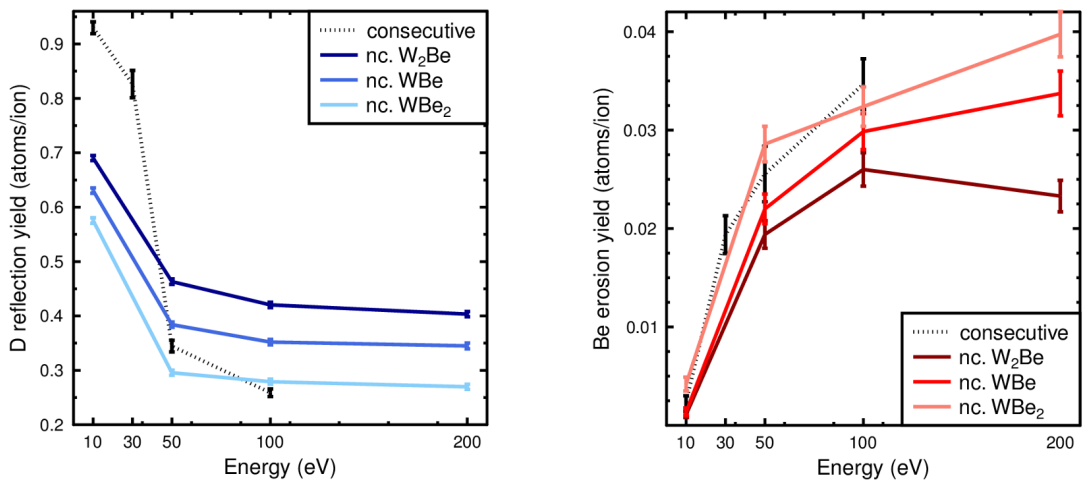

Figure 6. D reflection (left) and Be erosion (right) yield as function of the ion energy for D impacts on W-Be mixtures, cumulatively (dashed, consecutive irradiation) and non-cumulatively (solid).

below, 3.2.2).

3.2.2. Depth profiles after the consecutive Be-D irradiation The consecutive irradiation led to similar depth profiles as those obtained in the simultaneous irradiation at the lowest energies ($10 - 30$ eV; Fig. 7 left) with D located at the topmost surface, above the Be-rich mixed layer. However, at higher energies ($50 - 100$ eV; Fig. 7 right) the D clustered within or beneath the mixed W-Be layer, shown as a sharp peak in the depth profiles. The D clusters grew by the high D flux and invariant implantation depth (i.e., no Be layer grew while D was implanted), which could lead to bubble formation under these high irradiation fluxes.

3.2.3. Layer erosion by the consecutive Be-D irradiation Also the consecutive impacts led to the erosion of mixed layers, although showing different characteristics when compared to the simultaneous irradiation. On one hand, the Be sputtering yields were lower (Fig. 6) in the present case than in the simultaneous irradiation. The mixed W-Be layer used for consecutive Be-D irradiation was repeatedly quenched prior to the D impacts, thus being more stable. On the other hand, the Be erosion by consecutive impacts increased with the energy instead of peaking at lower energies, as all the cases used the same cell with a high Be surface concentration ($\sim 80\%$). These erosion yields are also similar to those from crystalline Be under similar irradiation conditions [27, 28]. Only at 100 eV the erosion by consecutive Be-D irradiation becomes higher. Within this physical sputtering regime, an amorphous surface may show a higher sputtering yield due to the lower surface binding energy. Very similar yields resulted also from the

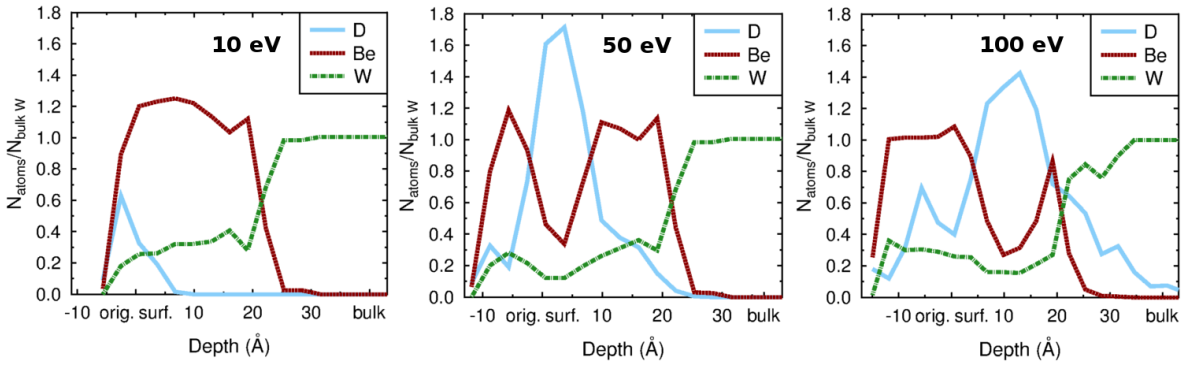

Figure 7. The D (blue), Be (red) and W (green) depth profiles after the consecutive irradiation, for 3000 cumulative D impacts, at 10 eV (left), 50 eV (centre) and 100 eV (right), on the mixed W-Be layer. The zero is located at the original surface of the W-Be mixture and the positive axis towards the bulk. The depth profiles are normalized to the atomic density of the original cell (BCC W lattice) and calculated every 3.1 Å (layer width in depth), to obtain a flat profile for bulk W. The statistical errors – not shown for clarity – lay between 0.005 and 0.09, as calculated for the lowest and highest concentrations, respectively.

non-cumulative irradiation, which were also performed using amorphous substrates.

Further, a wide range of molecules were found to sputter due to the consecutive Be-D irradiation. The D_2 molecule reflection (Fig. 8 left) showed a similar trend as for the simultaneous impacts (Fig. 5) with an even larger fraction of D emitted as D_2 in the present case. In contrast, the BeD erosion peak shifted to slightly higher energies ($\sim$ 50 eV, Fig. 8 right) when compared to the simultaneous irradiation (Fig. 5). Only the D impacts contribute to the BeD erosion in the present case, thus needing a higher energy for molecule sputtering than when Be is present among the projectiles. The Be and BeD erosion yields are very similar to those from the D irradiation of crystalline Be surfaces [27], and other similar species (BeD_2,BeD_3 and Be_2D_2) also showed the same trend.

3.3. Comparison to experiments and other simulations

3.3.1. Depth profiles The MD and experimental [5] Be depth profiles agreed on that a Be layer of $\sim$2 nm was deposited at 50 eV. The experimental fluence was higher than in our simulations, but it balanced out with the higher Be concentration in MD ($2 - 66\%$ Be), when compared to the experimental range ($0.1 - 2.5\%$ Be). Other computational erosion-deposition studies (using the EDDY code [9]) also agreed with this outcome, further showing an increase on the deposited layer when increasing the Be seeding rate and lowering the irradiation energy.

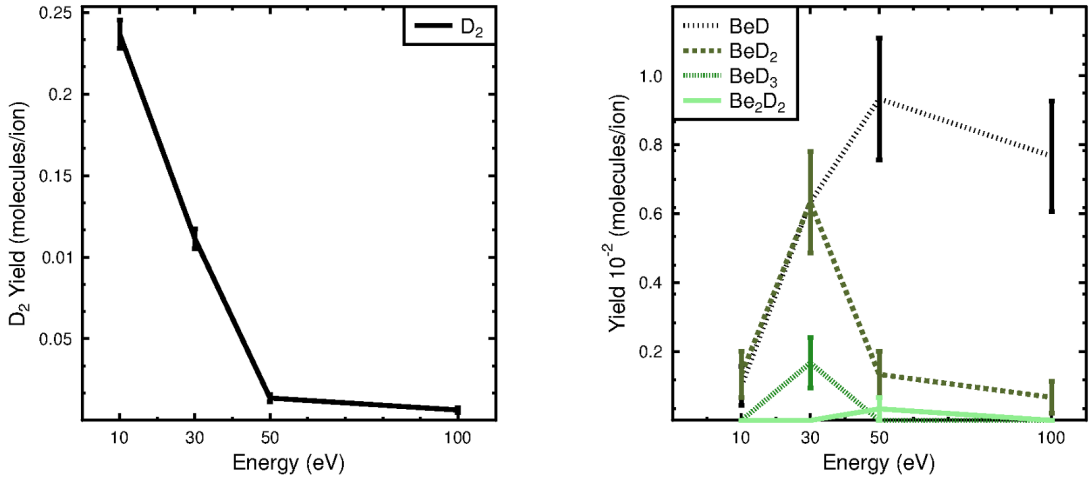

Figure 8. Be_nD_m molecule erosion yields as a function of the impacting energy, after 3000 cumulative D impacts on the mixed W−Be surface (consecutive irradiation).

3.3.2. Reflection and erosion rates The D reflection yield trends in experiments and MD agreed, with both showing an increase in the D implantation with the Be concentration [5, 8] at large enough seeding rates ($\geq$ 2.5% Be) for Be deposition. This layer growth leads to retention (in experiments) or implantation (in MD) yields exceeding those found in pure W or thin W-Be deposited on W. However, this statement must be taken carefully as the Be concentrations and time-scales differ between the experiments and MD ($0.1 - 2.5\%$ vs $2 - 66\%$ and ns vs s, respectively).

In contrast, our calculations disagreed with the outcome from the EDDY code on the impacting energy and Be seeding rate dependence of the D reflection yields [9]. These differences may be explained by i) the different irradiation energies, as monoenergetic impacts were modelled in MD, whereas plasma temperatures were given in EDDY, with a Boltzmann distribution of velocities; and ii) the binary collision approximation (BCA) like model used in EDDY, as at low energies BCA calculations have shown considerably different D reflection yields from W-Be mixed materials when compared to MD [11].

On the other hand, the Be deposition yields in the present MD work and EDDY calculations agreed when varying the impacting energy and seeding rate, especially at high Be concentrations. In general, both of these and previous studies [12] concluded that Be deposition on W at low energies lowered the Be reflection yields, further enhancing Be layer growth.

These three studies also showed consistent results regarding the substrate erosion, showing that Be seeding leads initially − at low Be fluences − to higher W erosion yields than for pure D irradiation. However, at higher fluences the sputtering is suppressed by Be layer deposition. The W sputtering yields in MD and EDDY calculations were in quantitative agreement.

3.3.3. D Bubble suppression The experimental result highlighted the D bubble inhibition in W due to the Be-seeding of the D plasma [5, 7]. The authors in Ref. [5] suggested several mechanisms for such an effect.

On one hand, the mixed Be-W layer resembles a Be surface rather than a W one, with a thickness of the order of the D implantation depth (a few nm). As no blisters have been observed experimentally in Be exposed to D plasmas, they would neither be expected in the deposited Be-rich layers. Our work supports this idea, as both the Be layer formation and D implantation within the deposited Be-W layer were seen in the simulations. Further, during the simultaneous D-Be irradiation the D got implanted as the Be layer grew. Together with the diffusion effects at experimental scales, it would be expected to prevent the D pile up to a particular depth, as seen for the consecutive irradiation in MD (3.1.2). Note that the clustering observed for consecutive Be-D irradiation is strongly related to the flux used in the MD simulations, 4-5 orders of magnitude higher than in experiments.

On the other hand, the authors in Ref. [5] also hint that the presence of a Be layer within the D implantation depth would reduce the stress in the W matrix caused by the D supersaturation present during the pure D irradiation. As reported in Section 3.1.1, our simulations showed the edge dislocation planes that resulted from the D supersaturation and the consequent stress fields, only at low Be fluences, supporting this mechanism to suppress the bubble formation.

4. Conclusions

We presented a Molecular Dynamics study of D plus Be irradiation of W surfaces. A wide range of cases were simulated: consecutive and simultaneous irradiation, for cumulative and non-cumulative impacts, and at projectile composition and impacting energy ranges relevant for fusion plasma-wall interactions. For the simultaneous irradiation, a wide range of structures formed such as edge dislocation planes, W amorphization and Be layer deposition. The Be sticking and D implantation increased with the Be fraction at low energies due to the Be layer formation. Both yields converged at higher energies. These characteristics were also shown in the depth profiles. Further, we confirmed that W was sputtered by Be, although the erosion was partially suppressed by the mixed layer formation. The balance between the Be concentration at the topmost surface and the projectile energy determined the Be erosion patterns and yields. A wide range of molecules were also sputtered: metal dimers (Be_2, BeW) sputtered physically and chemically; a large fraction of the D is reflected as D_2, showing that it is not a purely collisional process; and a high BeD erosion yield was found, peaking at low energies ($\sim$ 30 eV). On the other hand, the consecutive irradiation at the lowest energies showed similar implantation characteristics as for the simultaneous irradiation with a high Be fraction. In contrast, at higher energies the D clustered in or beneath the pre-deposited Be-W layer. Further, the Be erosion increased with the projectiles' energy and only the

D impacts on a Be-rich surface contributed to the BeD erosion, peaking at $\sim$ 50 eV. The yields for similar species showed the same trend.

5. Acknowledgments

This work, supported by the European Communities under the contract of Association between EURATOM/Tekes, was carried out within the framework of the European Fusion Development Agreement (EFDA). The views and opinions expressed herein do not necessarily reflect those of the European Commission. We acknowledge financial support from the National Graduate School in Materials Physics in Finland.

[1] ITER Physics Basis Editors, ITER Physics Expert Group Chairs, Co-Chairs, ITER Joint Central Team, and Physics Integration Unit, 1999.

[2] H. Okamoto and L. E. Tanner. Phase diagrams of binary tungsten alloys, 1991. Indian Institute of Metals, Calcutta.

[3] R.P. Doerner, M.J. Baldwin, and R.A. Causey. Beryllium-tungsten mixed-material interactions. *Journal of Nuclear Materials*, 342(1-3):63 – 67, 2005.

[4] R P Doerner, M Baldwin, J Hanna, Ch Linsmeier, D Nishijima, R Pugno, J Roth, K Schmid, and A Wiltner. Interaction of beryllium containing plasma with iter materials. *Physica Scripta*, 2007(T128):115, 2007.

[5] R.P. Doerner, M.J. Baldwin, D. Nishijima, J. Roth, and K. Schmid. Impact of beryllium surface layers on deuterium retention in tungsten. *Journal of Nuclear Materials*, 415(1, Supplement):S717 – S720, 2011. Proceedings of the 19th International Conference on Plasma-Surface Interactions in Controlled Fusion.

[6] M.J. Baldwin, R.P. Doerner, D. Nishijima, D. Buchenauer, W.M. Clift, R.A. Causey, and K. Schmid. Be-w alloy formation in static and divertor-plasma simulator experiments. *Journal of Nuclear Materials*, 363-365(0):1179 – 1183, 2007. Plasma-Surface Interactions-17.

[7] M.J. Baldwin, R.P. Doerner, D. Nishijima, K. Tokunaga, and Y. Ueda. The effects of high fluence mixed-species (deuterium, helium, beryllium) plasma interactions with tungsten. *Journal of Nuclear Materials*, 390-391:886 – 890, 2009. Proceedings of the 18th International Conference on Plasma-Surface Interactions in Controlled Fusion Device.

[8] G. De Temmerman, M.J. Baldwin, R.P. Doerner, D. Nishijima, and K. Schmid. An empirical scaling for deuterium retention in co-deposited beryllium layers. *Nuclear Fusion*, 48(7):075008, 2008.

[9] Shinji Ebisu, Kaoru Ohya, and Tetsuo Tanabe. Dynamic erosion and deposition on carbon and tungsten due to simultaneous bombardment with deuterium and beryllium ions in plasmas. *Fusion Engineering and Design*, 81(1-7):253 – 258, 2006. Proceedings of the Seventh International Symposium on Fusion Nuclear Technology, ISFNT-7 Part AProceedings of the Seventh International Symposium on Fusion Nuclear Technology.

[10] W. Eckestein, R. Dohmen, A. Mutzke, and R. Schneider. Sdtrimsp: A monte-carlo code for calculating collision phenomena in randomized targets. *IPP Reports*, (12/3), 2007.

[11] A. Lasa, K. Schmid, and K. Nordlund. Modelling of wbe mixed material sputtering under d irradiation. *Physica Scripta*, 2014(T159):014059, 2014. Proceedings of the 14th International Conference on Plasma-Facing Materials and Components for Fusion Applications.

[12] A. Lasa, K. Heinola, and K. Nordlund. Atomistic simulations of be irradiation on w: Mixed layer formation and erosion. *Nuclear Fusion*, 54(083001), 2014.

[13] C Björkas, D Borodin, A Kirschner, R K Janev, D Nishijima, R Doerner, and K Nordlund. Molecules can be sputtered also from pure metals: sputtering of beryllium hydride by fusion plasma-wall interactions. *Plasma Physics and Controlled Fusion*, 55(7):074004, 2013.

[14] A. Wiltner and Ch. Linsmeier. Formation of a surface alloy in the beryllium-tungsten system. *Journal of Nuclear Materials*, 337-339(0):951 – 955, 2005.

[15] A. Wiltner, F. Kost, S. Lindig, and Ch. Linsmeier. Structural investigation of the be-w intermetallic system. *Phys. Scr.*, T128:133–136, 2007.

[16] T. Ahlgren, K. Heinola, K. Vortler, and J. Keinonen. Simulation of irradiation induced deuterium trapping in tungsten. *J. Nucl. Mater.*, 427(1-3):152–161, 2012.

[17] A. Kirschner, V. Philipps, J. Winter, and U. Kogler. Simulation of the plasma-wall interaction in a tokamak with the Monte Carlo code ERO-TEXTOR. *Nucl. Fusion*, 40(5):989–1001, 2000.

[18] K. Schmid, M. Reinelt, and K. Krieger. An integrated model of impurity migration and wall composition dynamics for tokamaks. *J. Nucl. Mater.*, 415(1, S):S284–S288, 2011. 19th International Conference on Plasma-Surface Interactions in Controlled Fusion Devices (PSI), Univ Calif, Gen Atom, San Diego, CA, MAY 24-28, 2010.

[19] K. Nordlund, 2010. PARCAS computer code. The main principles of the molecular dynamics algorithms are presented in [29, 30]. The adaptive time step and electronic stopping algorithms are the same as in [31].

[20] C. Björkas, K. O. E. Henriksson, M. Probst, and K. Nordlund. A be-w interatomic potential. *J. Phys.: Condens. Matter (fast track communication)*, 22:352206, 2010.

[21] T. Alhgren, K. Heinola, N. Juslin, and A. Kuronen. Bond-order potential for point and extended defect simulations in tungsten. *American Institute of Physics*, 107:033516, 2010.

[22] K. Vörtler and K. Nordlund. Molecular dynamics simulations of deuterium trapping and re-emission in tungsten-carbide. *J. Phys. Chem. C*, 114:5382–5390, 2010.

[23] J.M. Ziegler. The stopping and range of ions in matter. http://www.srim.org/.

[24] A. Lasa, C. Björkas, K. Vörtler, and K. Nordlund. Md simulations of low energy deuterium irradiation on w, wc and w_2c surfaces. *Journal of Nuclear Materials*, 429(1-3):284 – 292, 2012.

[25] C. Björkas and K. Nordlund. Variables affecting simulated be sputtering yields. *Journal of Nuclear Materials*, 439(1-3):174 – 179, 2013.

[26] E. Safi, C. Björkas, A. Lasa, and K. Nordlund. Molecular dynamics simulation of deuterium irradiation on beryllium surfaces at different temperatures, 2013. personal communication.

[27] C Björkas, K Vörtler, K Nordlund, D Nishijima, and R Doerner. Chemical sputtering of be due to d bombardment. *New Journal of Physics*, 11(12):123017, 2009.

[28] M. Mehine, C. Björkas, K. Vörtler, K. Nordlund, and M.I. Airila. Modelling the erosion of beryllium carbide surfaces. *Journal of Nuclear Materials*, 414(1):1 – 7, 2011.

[29] K. Nordlund, M. Ghaly, R. S. Averback, M. Caturla, T. Diaz de la Rubia, and J. Tarus. Defect production in collision cascades in elemental semiconductors and fcc metals. *Phys. Rev. B*, 57(13):7556–7570, 1998.

[30] M. Ghaly, K. Nordlund, and R. S. Averback. Molecular dynamics investigations of surface damage produced by kev self-bombardment of solids. *Phil. Mag. A*, 79(4):795, 1999.

[31] K. Nordlund. Molecular dynamics simulation of ion ranges in the 1 – 100 kev energy range. *Comput. Mater. Sci.*, 3:448, 1995.